JOURNAL OF PROPULSION AND POWER
Vol. 19, No. 4, July–August 2003

Computational Fluid Dynamics Analysis of the Central Institute of Aviation Motors/NASA Scramjet

Carlos G. Rodriguez*
Allied Aerospace, Hampton, Virginia 23681

The flight test of the Central Institute of Aviation Motors/NASA scramjet was numerically analyzed. The flowpath was divided into inlet and burner sections and solved sequentially. Initial simulation of the inlet at high-speed conditions failed to describe the behavior of the data, which indicated the presence of separated flow near the throat. A qualitative analysis of low-speed operation showed inlet unstart and subsequent hysteresis effects that reproduced the main features of the flow revealed by the data. Simulation of the burner captured the dual-mode operation apparent in the data; calculated pressures somewhat underpredicted measured values. Effects of grid convergence, Schmidt number, chemistry models, and inlet nonuniformities were evaluated. In conclusion, current numerical tools seem adequate to anticipate qualitative effects of design and construction of scramjet engines. More work is needed to improve their accuracy, particularly in the field of turbulence modeling.

Nomenclature

M	=	Mach number
p	=	static pressure, Pa
Sc_T	=	turbulent Schmidt number
T	=	static temperature, K
T_0	=	total temperature, K
t	=	time, s
U	=	velocity, m/s
w	=	mass flow rate, kg/s
x	=	axial (streamwise) coordinate, m
y	=	vertical coordinate, m
y^+	=	dimensionless vertical turbulence coordinate
z	=	lateral coordinate, m
η_c	=	combustion efficiency
η_{mix}	=	mixing efficiency
μ_T/μ_L	=	turbulent/laminar viscosity ratio
ρ	=	density, kg/m^3
τ	=	turbulence intensity

Introduction

UNDER contract from NASA, Russia's Central Institute of Aviation Motors (CIAM) designed and built an axisymmetric, dual-mode scramjet engine. On 12 February 1998, this engine flew on the nose of a modified SA-5 missile. It was fueled with hydrogen for about 77 s and achieved the longest duration, dual-mode, scramjet-powered flight-test up to date.[1,2] The main program goals were to demonstrate supersonic combustion in actual flight, as well as to provide data for verification of scramjet design tools.[2] It was understood by both NASA and CIAM that axisymmetric configurations are not practical for operational systems. However, the data were still considered useful as partial validation of computational fluid dynamic (CFD) codes that are being considered or used in actual scramjet design.

The present work will describe the results obtained by application of one of these codes to the simulation of the CIAM scramjet experiment. Previous analysis of this experiment (to be described in more detail in a later section) either was limited to predicting the performance of the inlet design before the flight tests or did not include all of the characteristics of the test itself. The present numerical analysis, for the first time, models the as-built engine under the actual conditions of the flight test.

Flight Test

This section will summarize the CIAM scramjet experiment. It will concentrate on those aspects of the experiment that had a direct impact on the numerical simulation. Further information may be found in Refs. 1 and 2.

The design layout of the engine is shown in Fig. 1. It includes 1) an external/internal, axisymmetric, Mach-6 inlet; 2) a burner section with three fuel-injection stages; and 3) an expansion section with a partial nozzle. Except for the external inlet, most of the engine consists of an annular duct between the body of the engine and an external cowl. This cowl is held in place by two sets of struts.

The external inlet begins at the nose tip, which incorporates a pitot probe. The body itself consists of three conical segments with increasing half-angles. The internal inlet starts at the location of the blunt cowl lip. Body-side expansions and cowl-side compressions are used to turn the flow parallel to the body centerline by the time it reaches a diverging isolator, upstream of the first row of injectors.

The burner consists of three injector stages, denoted 1, 2, and 3 in Figs. 1b and 1c. Each stage has 42 injectors; the injectors of stages 1 and 2 are aligned and interdigitated with those of stage 3. Stages 1 and 3 are located near each of the two body-side cavities, whereas stage 2 is located at the cowl step. Hydrogen fuel was intended to be injected through all three stages. Stages 2 and 3 were to operate during most of the flight regime; stage 1 was supposed to operate above Mach 5, when supersonic combustion was expected.

As mentioned before, two sets of struts hold the engine together; each set consists of four struts. The first set is placed at the internal inlet. These struts have a small cross section and, presumably, have very little impact on the flow in the region. The second set is located toward the end of the engine, near the exit-nozzle throat. These struts have a large cross section. At this axial location, the cowl expands to compensate for the resulting area blockage. The cowl ends by opening up into an exit nozzle.

During manufacture of the engine, the internal flowpath was altered due to structural reinforcements, weld beads, and surface deformation resulting from the welding. These alterations reduced the inlet throat area and likely resulted in increased pressure losses. There is still considerable uncertainty regarding the final configuration. To add to this geometry uncertainty, posttest inspection of the engine showed combustor-liner deformations[2]; these deformations have not been quantified. In any case, the as-built pretest flowpath (including manufacturing departures from design), based on the best information available, was used for the present calculations.

Received 22 August 2002; revision received 26 January 2003; accepted for publication 5 February 2003.

*Senior Engineer, General Applied Science Laboratories Division, 6 North Dryden, Building 1298, Mail Stop 353X. Member AIAA.

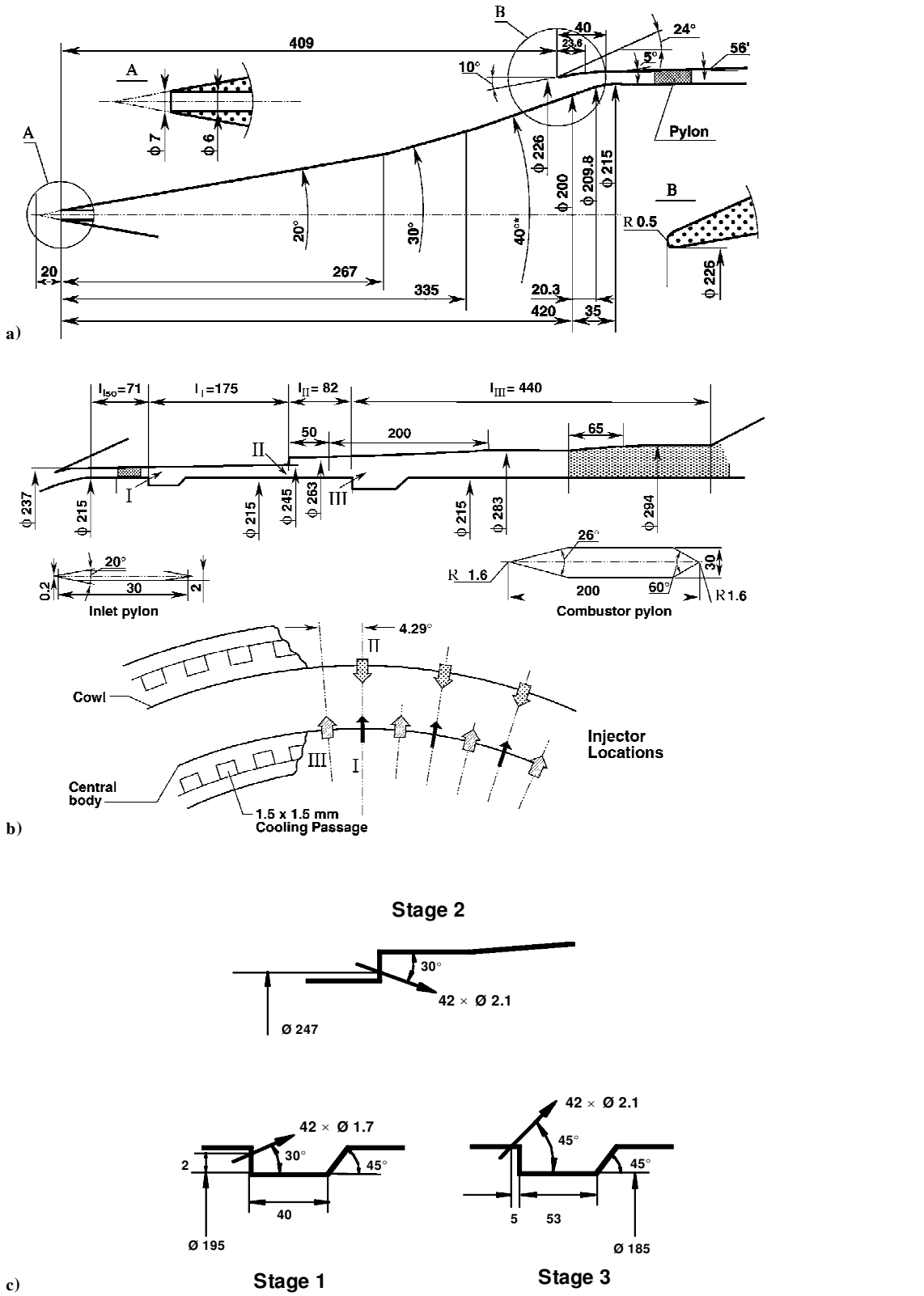

Fig. 1 Inlet and combustor design geometry (units in millimeters, ϕ denotes diameter): a) inlet, b) combustor, and c) injection stages (courtesy of R.T. Voland).

A brief description of the flight test follows. While the booster was still burning, fuel addition took place within the scramjet (approximately 38 s into the flight) at a flight Mach number of 3.5. The maximum velocity condition occurred at booster burnout, at a Mach of 6.4 (around 56 s). After burnout, the scramjet/missile combination followed a ballistic trajectory, with increasing altitude (and decreasing dynamic pressure) until a maximum altitude was reached (90 s). Afterward, dynamic pressure increased until flight termination (115 s).

Several anomalies and deviations from planned flight-test conditions occurred. First, the test took place at an altitude lower than anticipated. In particular, the maximum velocity condition occurred at 21.6 km, rather than 24 km. The resulting dynamic pressure and mass inflow were double the design values. Furthermore, an apparent failure in the fuel control system resulted in excessive fuel flow rate and engine unstart for about 12 s. The control system responded by drastically reducing the fuel flow rates of stages 2 and 3.

The engine restarted at about 50 s (Mach 5.0). However, the possible presence of large flow separation near the inlet throat caused the controls to keep stage 1 shut. As a result, combustion took place with only stages 2 and 3 active.

Previous Work and Present Approach

An analysis of the operation of the inlet design at the planned test conditions of Mach 6.5 and 26 km of altitude was done by Hawkins.[3] The analysis predicted inlet start in accordance to the Kantrowitz criterion and found only small separation bubbles at shock-impingement locations. Gaffney and Sanetrik (unpublished report, 1999) performed a CFD analysis of the full engine using the VULCAN code. The design geometry and planned freestream conditions at the maximum velocity point were used. The total fuel flow rate was similar to the experiment. To reduce computational expense, the entire flow was assumed axisymmetric. The rings of injector holes were replaced by axisymmetric slots of equivalent total area. Their calculated Mach contours within the burner suggest that the average Mach was subsonic, or nearly so.

The present work considers the CIAM flight test as it actually occurred. Some early results were reported elsewhere.[4,5] As mentioned before, the as-built geometry will be modeled. No attempt was made to account for possible in-flight deformation. The operating conditions chosen for analysis correspond to the maximum velocity point in the flight-test trajectory. As explained before, only stages 2 and 3 actually worked at the chosen operating condition. Therefore, for the purposes of this paper, "inlet" will denote the domain from a point upstream of the nose to a section in the duct just upstream of stage 2. The remaining duct will be considered the "burner." Note that, with these definitions, the inlet throat will be the minimum area just ahead of stage 1 injectors. The inlet and burner were intended to be solved separately and sequentially, with the exit conditions for the inlet to be used as inlet conditions for the burner. This approach had to be altered for reasons that will become clear later in the paper.

The VULCAN code was chosen for the present investigation. VULCAN is a general purpose CFD code that can solve the Reynolds-averaged Navier–Stokes equations. It has a wide array of physical, turbulence, and chemistry models available. A full description may be found in the literature.[6] The specifics of its application to the present work will be described throughout the paper.

Inlet

Solution Procedure

Because the inlet geometry (not accounting for stage 1 injectors) is axisymmetric, the axisymmetric form of the governing equations was solved with VULCAN for the obvious computational benefits. The actual grid was two dimensional, with approximately 192,000 control volumes (CV) divided among 15 blocks to facilitate the use of VULCAN's message passing interface (MPI) capabilities; 100 CVs were used along the duct height. The block configuration can be seen in Fig. 2a, with a detail of the grid in the neighborhood of the throat also shown Fig. 2b. The maximum wall spacing was less than 0.03 mm. The maximum y^+ was below 30 and occurred near the throat. The grid was mostly $C(0)$-continuous, except in the neighborhood of the cowl lip.

All inflow boundaries were set at freestream conditions, whereas extrapolation was used for outflow boundaries. Initially, the freestream conditions corresponded to the maximum velocity point in the trajectory (56.5 s into the flight). (See Table 1, in which the values for the turbulent intensity τ and viscosity ratio μ_T/μ_L were assumed.) Other freestream conditions were used, as will be explained later. All walls were modeled as no slip, with prescribed temperatures. The wall temperatures were taken from the measured values. For convenience, these were assumed to be stepwise constant along segments of the walls. No attempt was made to match the temperature value at the probe locations exactly; instead, the smoothest possible distribution was imposed.

The gas was approximated with a single-species, thermally perfect model of air available in VULCAN. To model the inviscid fluxes, Edwards' low-dissipation flux-split scheme[7] was used, together with third-order MUSCL extrapolation and Van Leer's limiter. Wilcox's 1998 k–ω model[8] was used for turbulence modeling, coupled with Wilcox's wall-matching functions at the solid walls. The turbulent Prandtl number was set at 0.90. Transition from laminar to turbulent flow was imposed at the first change in slope in the external inlet. This location is close to the one predicted by the usual conical-flow transition criteria[3] ($Re_\theta/M_e = 150$). In VULCAN, transition can be approximated by the use of laminar regions, or regions where source terms in the turbulence equations are turned off. Time integration was performed with the implicit diagonalized approximate-factorization scheme.[9] For most of the calculations, the local Courant–Friedrichs–Lewy (CFL) number was set at 2.0. The entire flowfield was solved elliptically, in spite of being mostly supersonic, in an attempt to capture all of the possible separation regions present in the domain. Note from the earlier discussion that the data suggest the presence of a large separation at the beginning of the internal inlet. Smaller separation bubbles may also be expected at shock-impingement locations. To reduce computational turnaround times, VULCAN's MPI capability was used. The calculations were done on an SGI Origin 2000 with 12 R10000 250-MHz processors. The resulting parallel ideal speedup was 11.40. Wall-time CPU was approximately 0.165 ms per CV per iteration. Determination of convergence by residual drop was not possible because of large oscillations in the residual. Most of these oscillations appear to occur in the first two blocks, around the pitot nose. Attempts to eliminate or reduce these oscillations were unsuccessful. Therefore, convergence was assumed when no change could be observed in the overall solution and wall-pressure trace. To accelerate convergence, grid sequencing was adopted with three sequences: coarse, medium, and fine. About 25,000 iterations were required (including about 7500 for the fine sequence). This procedure was also used to determine the degree of grid convergence, as will be shown in the results section.

Table 1 Freestream conditions at $t = 56$ s

Parameter	Value
T, K	203.5
p, Pa	3968
M	6.4
τ	.01
μ_T/μ_L	1.0

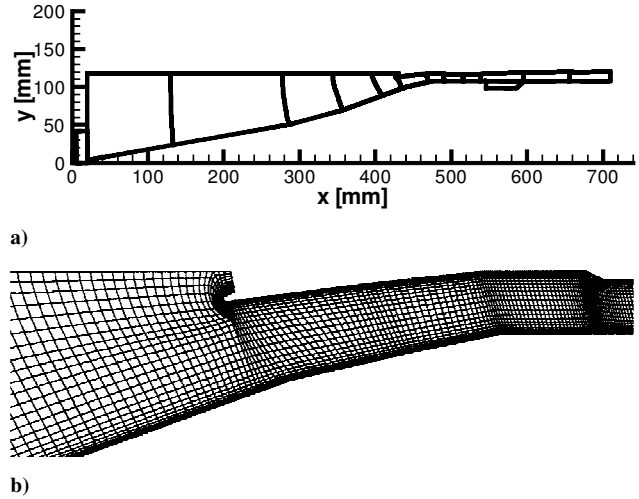

Fig. 2 Inlet grid: a) overall layout and block configuration and b) close-up view near the throat (every fourth grid line shown).

Results

The Mach contours for the inlet solution may be seen in Figs. 3a and 3b. A conical bow shock forms at the nose of the spike, detached

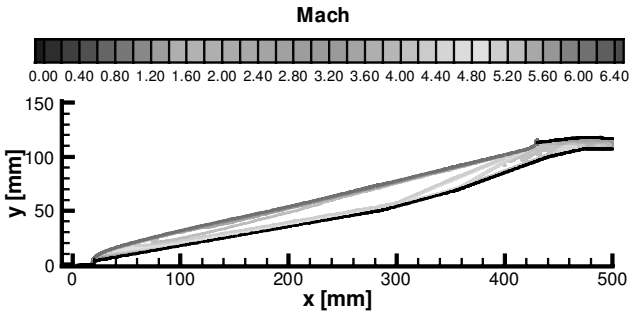

a) External inlet

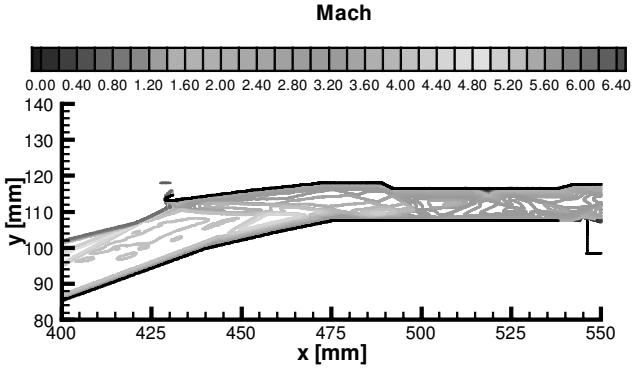

b) Detail of internal inlet

Fig. 3 Inlet, Mach contours.

from the body. Additional shock waves are formed at the compression corners of the external inlet. All of these shocks coalesce and end at the cowl lip (where another bow shock originates). A closer look at the internal inlet flowfield (Fig. 3b) shows the presence of small recirculation bubbles, particularly at the cowl lip and at the structural reinforcement. However, there is no evidence of the massive separation suggested by the data. The lack of separation is apparent in the wall-pressure trace (Fig. 4a), where the numerical distribution is compared with the data. The numerical results show a dip in the pressure trace in coincidence with the first body-side expansion (at about 440 mm). The data, on the other hand, show continuously increasing pressure at that point, which is consistent with boundary layer separation. Overall, the calculated pressures agree well with the data up to the point of the possible separation. Downstream from there, the predicted pressure levels are considerably lower than that which the data suggest. As for the pressure spikes, due to shocks created and reflected within the inlet, there are not enough data points to capture their location and strength. The calculated mass average Mach number at the exit is approximately 2.67, which is much higher than the value of 2.0 predicted by a one-dimensional analysis of the data.[2] The comparison of the body wall pressures for the medium and fine grid sequences is presented in Fig. 4b. The two solutions are sufficiently close for the fine sequence to be considered acceptable. Clearly, a straightforward approach fails to capture the behavior shown by the data.

Voland et al.[2] suggested that the inlet separation may have been caused by changes in the inlet geometry (with respect to the design) or by a hysteresis in the inlet starting process (or a combination of both). In the latter case, the massive separation created during the inlet unstart may have survived after the restart. Previous numerical experimentation performed by the present author[4] showed that, after an artificially induced inlet unstart, a separation region would remain in place near the throat even after removal of the cause. Furthermore, analysis of the flight data indicates that the inlet was unstarted before and up to the time fuel flow rate was turned on.[5] If this is the case, then a massive separation may have been created during low-speed operation (leading to inlet unstart), and, because of hysteresis, some of it remained in place even after reaching design flight conditions (and after the inlet restarted).

Table 2 Freestream conditions at several points in the flight trajectory

Parameter	Point in flight trajectory		
t, s	25	38	56
T, K	211	212	203.5
p, Pa	21710	9740	3960
M	2.57	3.51	6.4

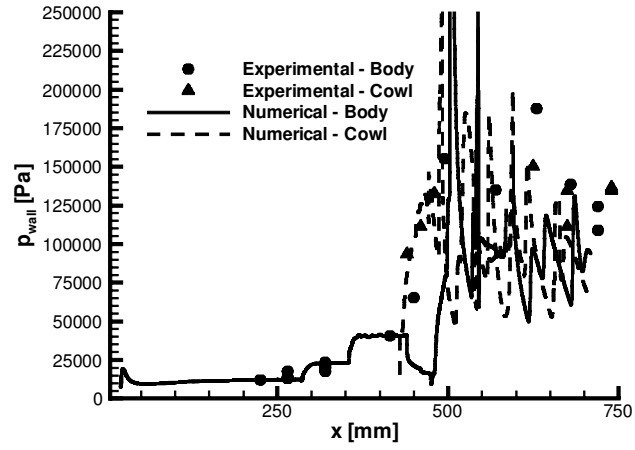

a)

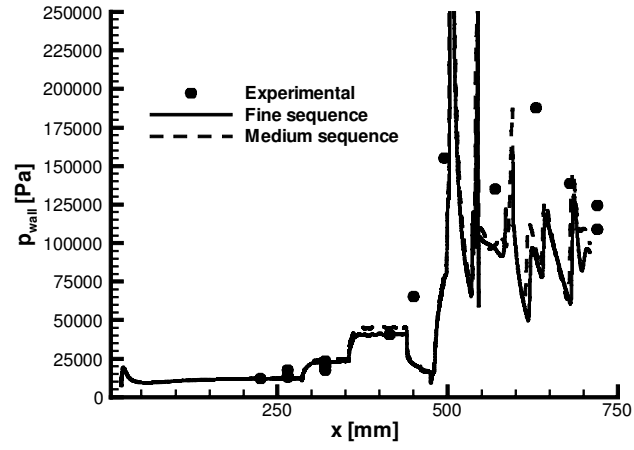

b)

Fig. 4 Inlet, wall pressures: a) body and cowl pressures and b) grid convergence for body pressures.

To have at least a qualitative insight into the phenomena, three points in the trajectory were run sequentially. (See Table 2.) In Table 2, $t = 38$ s corresponds to the point immediately before fuel addition. The first two conditions were run fully turbulent and with constant wall temperatures (at an average of the experimental data). The $t = 56$ s condition was run exactly as described before (but obviously with different initial conditions). Each condition was run for 15,000 iterations and with the same convergence criteria as before.

The results are shown in Figs. 5–7. At $t = 25$ s (Fig. 5) the shocks coming from the external inlet (not shown here) are far ahead of the inlet and do not interfere with the cowl lip. As a result, the shock coming from the lip is unobstructed and impinges on the body side, resulting in the separation of the boundary layer. (This process likely started earlier in the trajectory.) The recirculation region creates a shock that ends up ahead of the inlet. Therefore, the numerical simulation indicates that the inlet was unstarted under these flow conditions. The fair qualitative agreement with the data suggests that this was likely the case during the flight. By $t = 38$ s (Fig. 6) the inlet is still unstarted, as both data and CFD show. Note that, under these conditions, the numerical flow appeared to be highly transient, with the body–wall recirculation increasing and decreasing in size. Shown in Fig. 6 is the recirculation at its smallest.

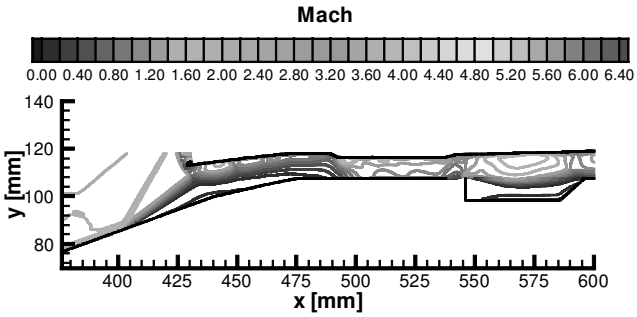

a)

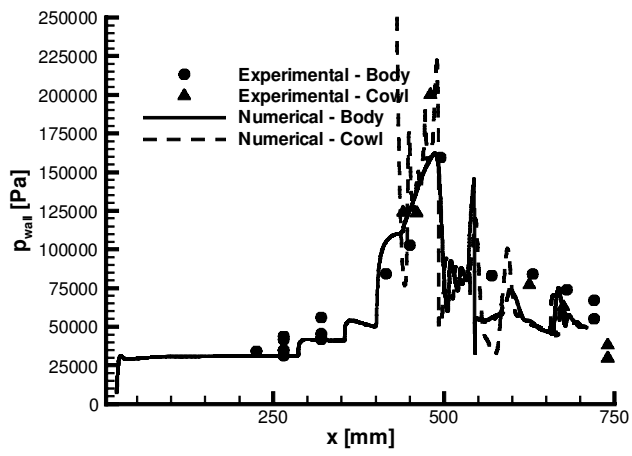

b)

Fig. 5 Inlet, $t = 25$ s: a) Mach contours and b) body pressures.

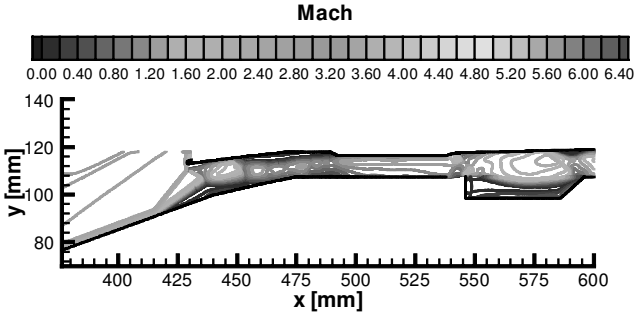

a)

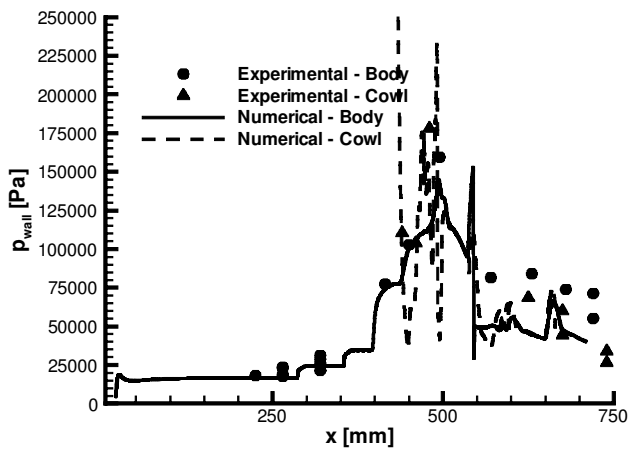

b)

Fig. 6 Inlet, $t = 38$ s: a) Mach contours and b) body pressures.

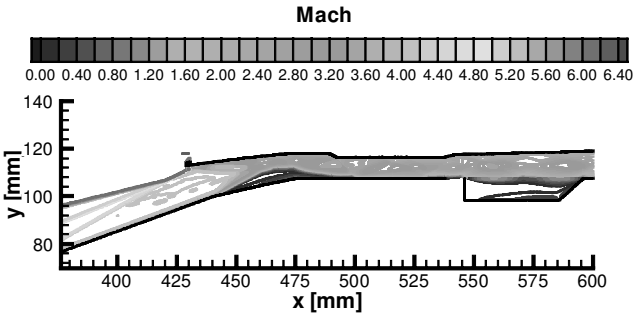

a)

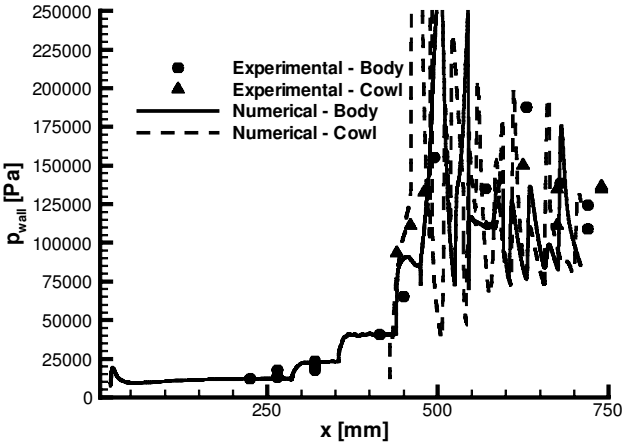

b)

Fig. 7 Inlet, $t = 56$ s: a) Mach contours and b) body pressures.

Finally, at the maximum velocity point of $t = 56$ s (Fig. 7) the inlet has restarted, but a recirculation region remains at the throat. This seems to be consistent with the data. There was a small unsteadiness associated with the recirculation shape, but without any major change in size. There is a better qualitative agreement with the pressure data, compared with the straightforward approach at the same conditions. (See Fig. 4.) However, the pressure levels are still low; the mass-averaged exit Mach number is about 2.40.

It is acknowledged that the procedure just outlined is, at best, a qualitative approximation to the full simulation of the flight trajectory, which would require a time-accurate calculation of the full engine. The theory presented was meant to provide a plausible explanation of the behavior shown by the data, which could not be reproduced by a more direct approach.

For reasons that will become clearer later in the paper, the last set of results was quantitatively inadequate to be used as inlet conditions for the burner calculations. Therefore, an attempt was made by means of an ad hoc procedure to create exit conditions that more closely resemble those of the data. Figure 8 shows the results when air at high pressure and low speed is injected to the flowfield of Fig. 7 to raise the pressure levels. Although the extent of the separation is overpredicted, the exit pressures are closer to the data than in the preceding case. The mass-averaged Mach number is about 1.90. These results will be used in some of the burner analysis that follows.

Burner

Solution Procedure

Burner calculations were done on a three-dimensional slice limited by the jet centerplanes between adjacent stage 2 and 3 injectors; this domain corresponds to about 4.3 deg of the annular combustor. (See Fig. 1b.) To simplify the grid generation, and because the resulting width was much smaller than the body radius, the domain was approximated as rectangular, with the jet centerplanes parallel to each other and normal to the body and cowl walls.

The grid was discretized into approximately 2.8 million CVs, distributed among 48 blocks (Fig. 9). The number of CVs ranged

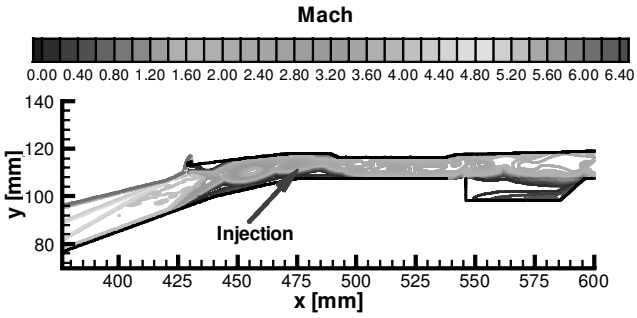

a) Mach contours

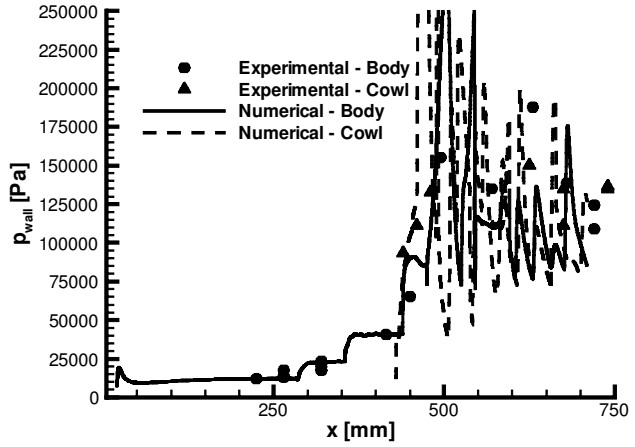

b) Body pressures

Fig. 8 Inlet, injection near the throat.

from 76 to 132 in the vertical direction, and from 28 to 36 laterally; the higher numbers correspond to the vicinity of the injectors. The wall spacing varied from 0.1 mm at the inlet to 0.5 mm toward the exit. The resulting y^+ was mostly under 100, except near the exit nozzle where the flow accelerated to supersonic conditions (as will be shown later) and where the y^+ could be as high as 200. The increase in y^+ with respect to the inlet calculations was necessitated by the considerably greater computational requirements of three-dimensional reacting flows. A grid-convergence analysis, to be shown later, suggests that these wall spacings are adequate to capture overall flow behavior. Non-$C(0)$ grid blocks were used throughout the geometry, especially near the injectors, to reduce computational effort. Note that the area increase immediately before the exit nozzle in the experimental configuration is missing from the computational domain. As mentioned before, this expansion was meant to compensate for the rear struts blockage. Because these struts are not being modeled, the area was held constant in the numerical simulation.

Unless otherwise noted, all calculations were done with the conditions and procedure to be described next (hereafter known as baseline conditions). At the jet centerplanes, symmetry boundary conditions were imposed. No-slip, prescribed temperature conditions were used at the walls, with the experimentally measured temperatures approximated in the same way as in the inlet. An extrapolation boundary condition was used at the exit. Hydrogen fuel was injected at sonic conditions through stages 2 and 3 and at the angles shown in Fig. 1c. The resulting mass flow rates gave an overall equivalence ratio of about 0.60. At the location of the injectors, fixed boundary conditions were imposed with the values of Table 3.

For the baseline condition, a uniform inlet was assumed, such that it gave the same mass flow rate, mass-averaged total temperature, and turbulence conditions as the inlet exit conditions for $t = 56$ s (Fig. 7) and a Mach number of 2.0. These conditions are summarized in Table 4. The uniform-profile assumption was a consequence of the quantitative limitations described in the preceding inlet analysis. The effects of nonuniform inlet profiles will be addressed hereafter.

Table 3 Injectant conditions

Parameter	Stage 2	Stage 3
M	1.0	1.0
T_0, K	716	771
T, K	597	642
U, m/s	1864	1934
ρ, kg/m^3	0.155	0.149
w, kg/s	0.042	0.042

Table 4 Inlet conditions for burner calculations

Parameter	Value
T_0, K	1632
ρ, kg/s	0.467
M	2.0
t	0.06
μ_T/μ_L	350

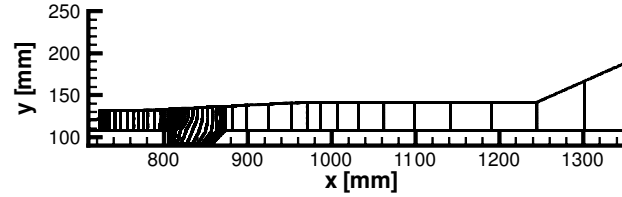

a)

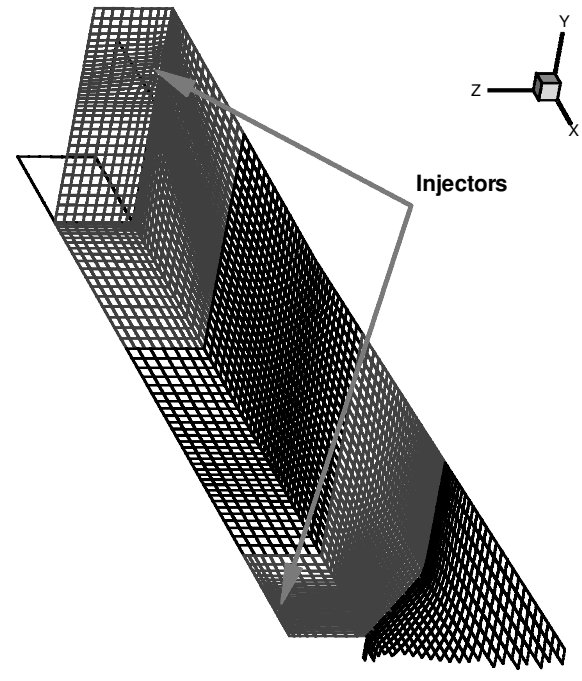

b)

Fig. 9 Burner grid: a) overall layout and block configuration and b) close-up view near the injectors (every fourth grid line shown).

The solution procedure was similar to the one employed for the inlet simulation; only those features that were different will be detailed in this section. The gas was assumed to be a mixture of thermally perfect gases. The chemistry model used was NASA Langley's 7-specie/7-reaction (7×7) model.[10] At the operating conditions, this model was difficult to autoignite; therefore, either a one-step reaction model or VULCAN ignition regions were used to initiate the reaction. The turbulent Prandtl and Schmidt numbers were set at 1.0. Turbulence modeling also used Wilcox's compressibility correction[8] to model Mach number effects on mixing. As before, a three-grid sequence was used for convergence acceleration. Maximum CFL was 5.0. Approximately 60,000 iterations were run, of

which about 40,000 corresponded to the fine sequence; convergence will be discussed in the next subsection. There were 48 R10000 400-MHz processors used, with a resulting ideal speedup of 47.0. Wall-time CPU was approximately 0.264 ms per CV per iteration.

Results

Figure 10a, shows the Mach contours for the vertical plane midway between the two injectors. A low-speed flow region begins at the step on the cowl wall and extends just past the cavity. The core flow is supersonic up to $x \sim 950$ mm, where it begins to deccelerate through a shock train to almost sonic conditions. This is confirmed by the mass-averagedone-dimensionalMach distribution(Fig. 10b). The flow finally reaccelerates to supersonic conditions at the nozzle exit. The extent of the reaction may be judged from the water contours and the axial distribution of efficiencies (Figs. 11a and 11b); η_{mix} and η_c are defined[11] as mixed fuel over total fuel, and reacted (water) fuel over total fuel, respectively (all evaluated at local axial planes). Most of the fuel from stage 2 appears to have mixed by the time it reaches the stage 3 axial location. Because of ignition delay, however, it starts to react shortly before that location, and appears consumed by the time it reaches the constant-area section ($x \sim 900$ mm). Stage 3 fuel, on the other hand, seems to start reacting in the constant section, contributing perhaps to the choking of the flow. All of the fuel is mixed, and almost all of it (94%) reacts by the time it reaches the exit.

Comparison of the calculated wall pressure traces with the data (Fig. 12) show that CFD somewhat underpredicts the pressures up to $x \sim 900$. Furthermore, it shows a reacceleration or supersonic region just downstream of the cavity, corresponding to the closing of the cowl-wall low-speed region. (This can also be seen in the one-dimensional average of Fig. 10b.) The data do not show reacceleration at that location. (There are too few data points to determine whether there was any reacceleration in the experiment.) Downstream from there, the numerical pressures recover their values before reacceleration and remain fairly constant (in coincidence with the subsonic region) until reaching the exit nozzle; the experimental pressures also appear constant but at a somewhat higher value. There was some unsteadiness in the fine-sequence solution between 800 and 900 mm, approximately. A fully steady-state solution was not achieved. The origin of this unsteadiness was most likely the recirculation region, and it resulted in changes in the pressure levels of about 10 kpa in this region. These values alternated for the last 25,000 iterations, and the results shown correspond to the lowest pressures.

The effects of grid sequencing (and, therefore, grid convergence) are shown in Fig. 13 for the body–wall pressures. There are small differences at the inlet and toward the exit; the maximum burner pressure seem to be the same for both grids. Overall, the two calculations are close enough, for a factor of eight in the number of CVs, to consider the solution to be grid converged. Because the medium

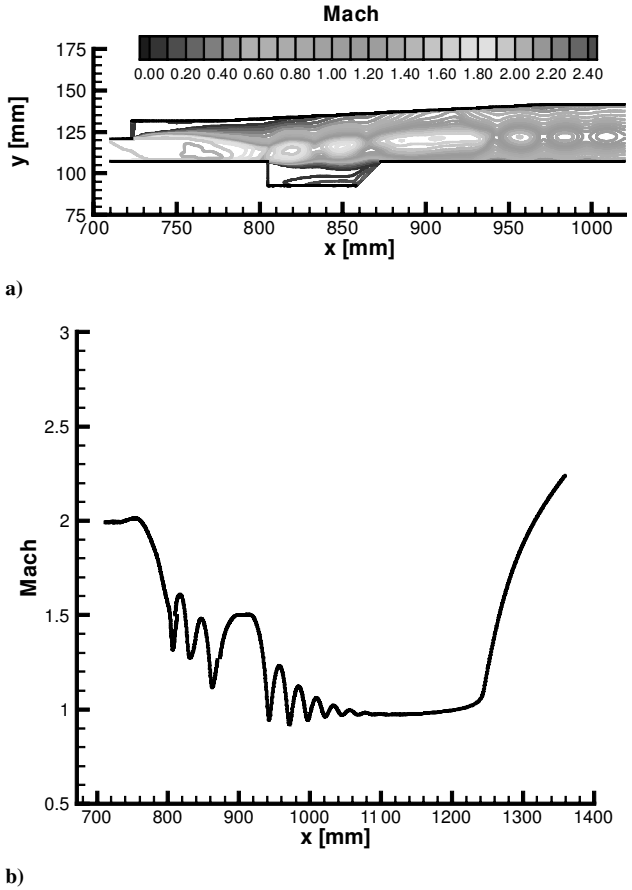

Fig. 10 Burner, Mach number distribution: a) centerplane Mach contours and b) one-dimensional mass-averaged Mach axial distribution.

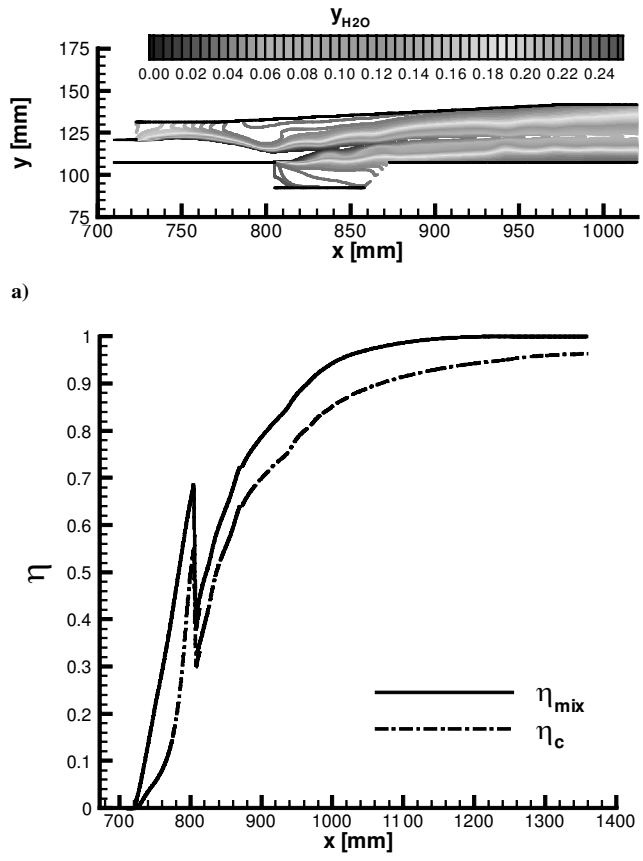

Fig. 11 Burner, heat-release: a) centerplane water mass-fraction contours and b) efficiency axial distribution.

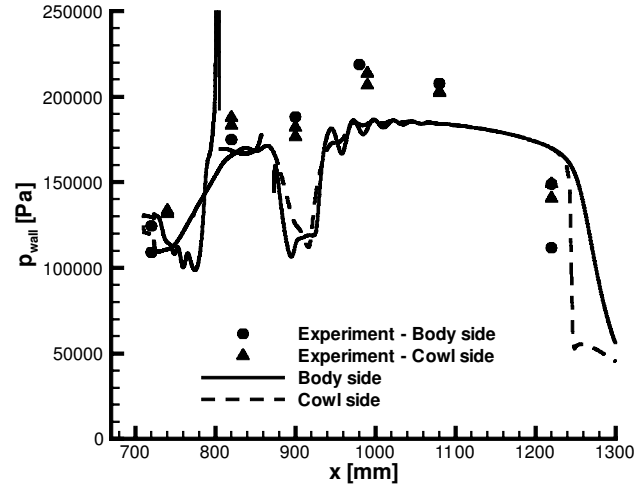

Fig. 12 Burner, body and cowl wall pressures.

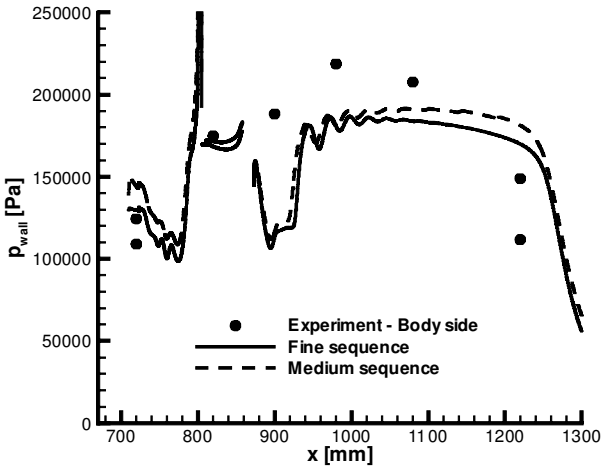

Fig. 13 Burner, body-side wall pressures for medium and fine grid sequences.

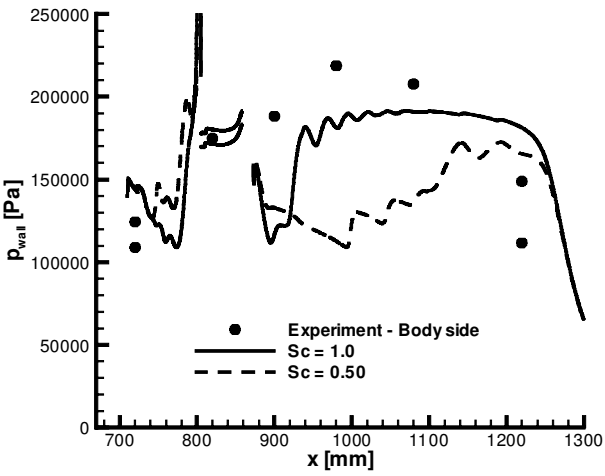

a)

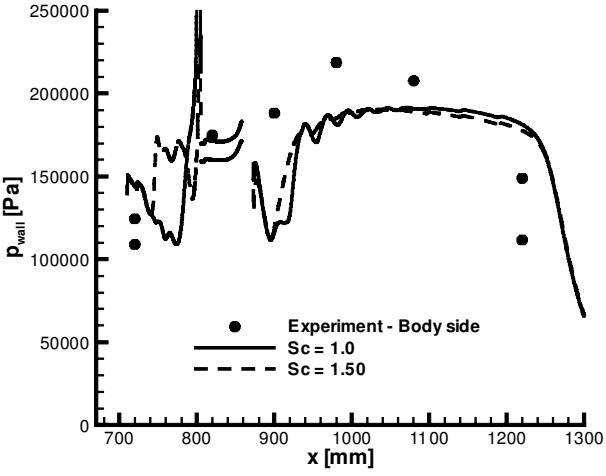

b)

Fig. 14 Burner, effects of turbulent Schmidt number on body-side wall pressures: a) $Sc_T = 0.50$ and b) $Sc_T = 1.50$.

sequence appears to give a qualitatively good solution, it was used to perform a series of parametric studies. In what follows, all results correspond to the medium sequence unless otherwise noted.

Lowering the turbulent Schmidt number (Sc_T) from 1.0 to 0.5 (Fig. 14a) and turning the compressibility correction off enhances the mixing and heat release. It also increases the pressure in the near field ($x < 800$ mm). However, it gives a much larger supersonic region and lower pressure after choking. It would seem that too much

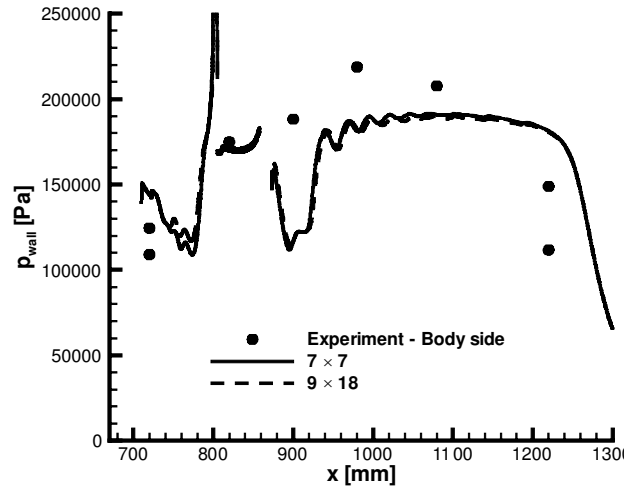

a)

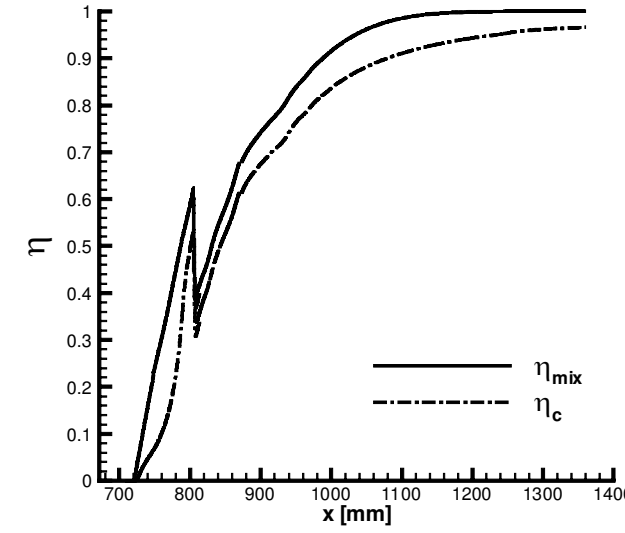

b)

Fig. 15 Burner, 9 × 18 chemistry model: a) body-side wall pressures and b) efficiency distributions.

heat release immediately after stage 3, that is, the expanding-area section, reduces the pressure levels in the constant-area section. Increasing the Sc_T to 1.50 (Fig. 14b) has less of an effect; the solution is actually very close to that of the $Sc_T = 0.50$ solution. Apparently, most of the heat-release should occur between injector stages and in the constant-area section to have a maximum effect on the pressure rise and better agreement with the data. Strong sensitivity of dual-mode combustion to turbulent transport coefficients has been reported in the literature.[12]

Switching from a 7 × 7 to a 9 × 18 chemistry model[10] (all other conditions left at their baseline values) does not appear to have a major impact on the solution (Fig. 15a). The efficiency distributions (Fig. 15b) are somewhat lower in the near field, but otherwise very close to the 7 × 7 model. The chemistry modeling does not seem to be as critical a factor as the mixing governed by the turbulence modeling.

The effects of nonuniform inlet profiles are addressed in Figs. 16 and 17. By the use of the exit conditions from the inlet calculations shown in Fig. 8, the Mach contours (Fig. 16) and wall pressures (Fig. 17a) are qualitatively similar to the corresponding ones with uniform inlets at similar averaged values. However, with an inlet profile whose mass-averaged Mach number is approximately 2.25, the results are dramatically different (Fig. 17b): The heat release appears to be insufficient to choke the flow. This is the reason why the solution from Fig. 7, with an even higher inlet Mach number, was considered inadequate for use in the burner calculations. In general,

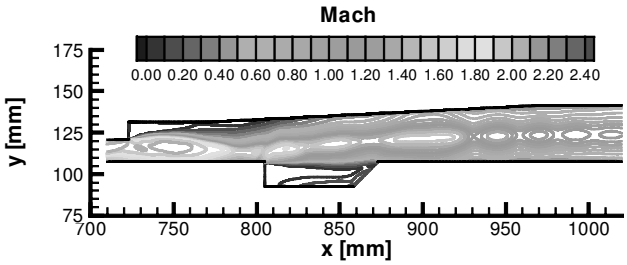

Fig. 16 Burner, centerplane Mach contours for nonuniform inlet profile ($M_{inlet} \sim 1.90$).

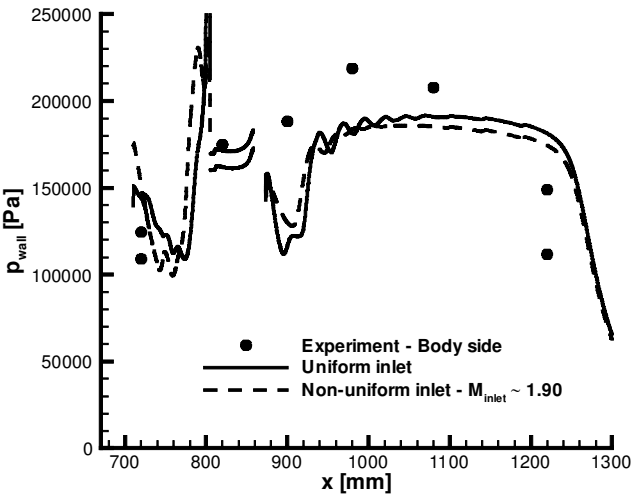

a)

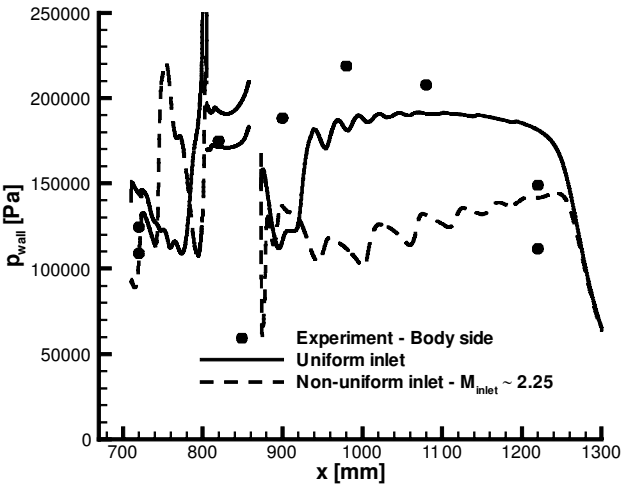

b)

Fig. 17 Body-side wall pressures for nonuniform inlet profiles: a) $M_{inlet} \sim 1.90$ and b) $M_{inlet} \sim 2.25$.

the performance of a scramjet combustor will depend on both bulk properties and profile shape at the inflow. However, under the present operating conditions, it appears that the average inlet properties have a greater impact than the details of the profile itself in determining the flow behavior within the burner, that is, choked or unchoked. Note again that the use of these approximations applied to the inlet conditions is necessitated by the difficulties in accurately modeling a partially restarted inlet.

Conclusions

The CIAM/NASA scramjet flight test was subjected to a CFD analysis. The data from the experiment show that the inlet was unstarted from a freestream Mach number of about 2.5 to about 5.0 (including the start of fuel injection). Even after restart, separated flow remained just ahead of the throat up to the Mach 6.4 condition being evaluated in the present paper.

CFD analysis performed at the Mach 6.4 condition suggests that the inlet would have started and operated as designed, without major flow separation. This result is not consistent with the data. A qualitative study starting from the Mach 2.5 conditions showed the presence of massive separation at low-speed conditions. At reaching Mach 6.4 conditions, the inlet restarted, but significant separation remained because of apparent hysteresis effects.

The separated flow in the inlet caused significant total pressure loss, lowering the combustor entrance Mach number from an expected value of about 2.7 to an actual value near 2.0. With this lower Mach inlet condition, the resulting CFD solutions somewhat underpredicted the measured flight wall pressure data. Both data and computations show the burner operating in a classical dual mode, with large regions of subsonic reacting flow dominating the combustor. The present analysis indicates that the fuel was completely mixed and that the combustion efficiency was 94% at the combustor exit.

The effects of the turbulent Schmidt number far outweight those of the chemistry model and inlet nonuniformities. Therefore, turbulence and transport models for the highly distorted combustor flow may need to be reassessed. The relaxation of the constant turbulent Schmidt number assumption should be a priority. As it stands, the present analysis showed that CFD is able to predict potential problems in a given design (and construction), to prevent them from occurring in an actual experiment or flight test.

Acknowledgments

This research was initially funded by NASA Grant NASW-4907 through the National Research Council, with C. R. McClinton as Technical Advisor. The author wishes to thank R. T. Voland, M. S. Smart, and A. H. Auslender for their help in providing the experimental data, as well as their suggestions and comments. R. L. Gaffney made available his unpublished report and gave useful advice. R. A. Baurle assisted with one-dimensional processing of numerical results. J. A. White continued to provide support in the use of the VULCAN code for this and other projects.

References

[1]McClinton, C., Roudakov, A., Semenov, V., and Kopehenov, V., "Comparative Flow Path Analysis and Design Assessment of an Axisymmetric Hydrogen Fueled Scramjet Flight Test Engine at a Mach Number of 6.5," AIAA Paper 96-4571, Nov. 1996.

[2]Voland, R. T., Auslender, A. H., Smart, M. K., Roudakov, A., Semenov, V., and Kopehenov, V., "CIAM/NASA Mach 6.5 Scramjet Flight and Ground Test," AIAA Paper 99-4848, Nov. 1999.

[3]Hawkins, R. W., "Computational Fluid Dynamics Analysis of Oversped Central Institute of Aviation Motors Scramjet at Mach 6.5," HNAG Rept. 96-1-071, NASA Langley Research Center, 1996.

[4]Rodriguez, C. G., "Computational Fluid Dynamics Analysis of the Central Institute of Aviation Motors/NASA Scramjet Engine (I): Inlet and Scramjet Analysis," HX Rept. HX-977, NASA Langley Research Center, 2001.

[5]Rodriguez, C. G., "Computational Fluid Dynamics Analysis of the Central Institute of Aviation Motors/NASA Scramjet Engine (II): Inlet Unstart and Restart," HX Rept. HX-978, NASA Langley Research Center, 2001.

[6]White, J. A., and Morrison, J. H., "A Pseudo-Temporal Multi-Grid Relaxation Scheme for Solving the Parabolized Navier–Stokes Equations," AIAA Paper 99-3360, Jan. 1999.

[7]Edwards, J. R., "A Low-Diffusion Flux-Splitting Scheme for Navier–Stokes Calculations," *Computers and Fluids*, Vol. 26, No. 6, 1997, pp. 635–659.

[8]Wilcox, D. C., *Turbulence Modeling for CFD*, 2nd ed., DCW Industries, La Canada, CA, 1998.

[9]Pulliam, T. H., and Chaussee, D. S., "A Diagonal Form of an Implicit Approximate-factorization Algorithm," *Journal of Computational Physics*, Vol. 39, Feb. 1981, pp. 347–363.

[10]Drummond, J. P., Rogers, R. C., and Hussaini, M. Y., "A Detailed Numerical Model of a Supersonic Reacting Mixing Layer," AIAA Paper 86-1427, June 1986.

[11]Rogers, R. C., "A Study of the Mixing of Hydrogen Injected Normal to a Supersonic Airstream," NASA TN D-6114, 1971.

[12]Eklund, D. R., Baurle, R. A., and Gruber, M. R., "Numerical Study of a Scramjet Combustor Fueled by an Aerodynamic Ramp Injector in Dual-Mode Combustion," AIAA Paper 2001-0379, Jan. 2001.